E46K α-synuclein pathological mutation causes cell-autonomous toxicity without altering protein turnover or aggregation

Ignacio Íñigo-Marco[a,b], Miguel Valencia[a,c,d], Laura Larrea[a], Ricardo Bugallo[a,b], Mikel Martínez-Goikoetxea[e], Iker Zuriguel[e], and Montserrat Arrasate[a,c,d,1]

[a]Neuroscience Program, Center for Applied Medical Research, University of Navarra, Pamplona 31008, Spain; [b]Graduate Program in Neuroscience and Cognition, School of Medicine, University of Navarra, Pamplona 31008, Spain; [c]School of Medicine, University of Navarra, Pamplona 31008, Spain; [d]Neuroscience Department Navarra Institute for Health Research, Pamplona 31008, Spain; and [e]Department of Physics and Applied Mathematics, School of Sciences, University of Navarra, Pamplona 31008, Spain

α-Synuclein (aSyn) is the main driver of neurodegenerative diseases known as "synucleinopathies," but the mechanisms underlying this toxicity remain poorly understood. To investigate aSyn toxic mechanisms, we have developed a primary neuronal model in which a longitudinal survival analysis can be performed by following the overexpression of fluorescently tagged WT or pathologically mutant aSyn constructs. Most aSyn mutations linked to neurodegenerative disease hindered neuronal survival in this model; of these mutations, the E46K mutation proved to be the most toxic. While E46K induced robust PLK2-dependent aSyn phosphorylation at serine 129, inhibiting this phosphorylation did not alleviate aSyn toxicity, strongly suggesting that this pathological hallmark of synucleinopathies is an epiphenomenon. Optical pulse-chase experiments with Dendra2-tagged aSyn versions indicated that the E46K mutation does not alter aSyn protein turnover. Moreover, since the mutation did not promote overt aSyn aggregation, we conclude that E46K toxicity was driven by soluble species. Finally, we developed an assay to assess whether neurons expressing E46K aSyn affect the survival of neighboring control neurons. Although we identified a minor non–cell-autonomous component spatially restricted to proximal neurons, most E46K aSyn toxicity was cell autonomous. Thus, we have been able to recapitulate the toxicity of soluble aSyn species at a stage preceding aggregation, detecting non–cell-autonomous toxicity and evaluating how some of the main aSyn hallmarks are related to neuronal survival.

alpha-synuclein | E46K mutation | serine 129 phosphorylation | neuronal death | autonomous toxicity

The abnormal accumulation of the presynaptic protein α-synuclein (aSyn) is the hallmark of a broad spectrum of neurodegenerative disorders collectively known as "synucleinopathies" (1). Mutations in the gene encoding aSyn (*SNCA*) are associated with familial forms of these diseases. For example, nonsynonymous point mutations and triplications of the *SNCA* gene are linked to autosomal dominant Parkinson's disease (PD), while gene duplication of the *SNCA* gene is sufficient to cause dementia with Lewy bodies (DLB) (2). Indeed, genome-wide association studies have identified the *SNCA* gene as one of the strongest risk loci in sporadic forms of PD (3, 4). Polymorphisms within the *SNCA* promoter increase PD susceptibility (5), and a PD-associated risk variant located in a distal enhancer of the *SNCA* gene regulates aSyn expression (6). Thus, aSyn would appear to play a central role in these pathologies, and enhanced aSyn expression may even be sufficient to cause familial forms of synucleinopathies and favor the onset of sporadic cases.

The molecular mechanisms by which aSyn causes neuronal death remain elusive. The aSyn protein is intrinsically disordered, existing predominantly as a monomer (7), although tetrameric conformations could exist in a dynamic equilibrium (8).

A misfolded conformation of aSyn monomers could be more prone to assemble into intermediate or oligomeric aSyn species, triggering fibrillization and their final aggregation into Lewy bodies (LBs), the pathological hallmark of synucleinopathies (9–11). The enhanced expression of WT aSyn may be sufficient to initiate this aggregation cascade. Similarly, pathological point mutations could contribute to aSyn aggregation by impairing protein degradation, thereby augmenting the steady-state protein levels and/or favoring the accumulation of aggregation-prone aSyn conformations. In vitro and in vivo studies suggest that aSyn mutations alter degradation pathways (i.e., chaperone-mediated autophagy) (12) and that they modulate aSyn aggregation (13). However, there is still no conclusive evidence about which are the toxic aSyn species (monomers, oligomers, or fibrillar/aggregated LBs) or how these toxic species contribute to neurodegeneration. When forming LBs, most aSyn is phosphorylated at serine 129 (S129) (14), a modification that might promote aggregation or that might occur after aSyn assembles into LBs. Despite much effort in cellular and animal models, it remains unclear how this hallmark relates to neurodegeneration (15).

In recent years, the hypothesis that pathological proteins spread from neuron to neuron has been proposed as a non–cell-autonomous mechanism to explain the progression of PD neurodegeneration. Toxic aSyn protein species could be secreted by

Significance

α-Synuclein (aSyn) plays a key role in neurodegenerative disorders known as "synucleinopathies." By tracking individual primary neurons overexpressing wild-type and mutant aSyn versions we have determined how pathological hallmarks like alterations in aSyn expression and stability, aggregation, or serine 129 phosphorylation (PS129) contribute to neuronal death. We have found that the E46K mutant displayed the highest toxicity. Neurotoxicity was independent of aggregation but correlated with PLK2-dependent PS129. Surprisingly, inhibiting PS129 did not affect neuronal survival, suggesting that this modification is an epiphenomenon. Finally, we set up an assay to score for cell-autonomous and nonautonomous toxicity. While we identified a minor non–cell-autonomous component restricted to proximal neurons, E46K toxicity was mostly cell autonomous.

cells and taken up by surrounding neurons, serving as a template to trigger the misfolding and aggregation of the endogenous protein in a prion-like manner (16). Consistent with this idea, aSyn of CNS origin has been detected in the cerebrospinal fluid of healthy individuals and persons with PD (17, 18). Overexpression of aSyn in neuronal models promotes aSyn release into the extracellular milieu (19, 20), and exogenous preformed aSyn fibrils injected into mouse brains can be taken up by neurons, promoting the aggregation of endogenous aSyn in these cells (21–24). Moreover, brain propagation with nonfibrillar aSyn protein species has also been observed in mice (25).

The spreading of toxic aSyn species could explain the ascending pattern of LB distribution in PD postmortem human brains: from the lower brainstem toward the pons, mesencephalon, and to the cortical regions at later stages of the disease (26). While this hypothesis has generated much interest, the involvement of aSyn-dependent, cell-autonomous mechanisms targeting neuronal populations at different stages during disease progression as a result of differential vulnerability has not been ruled out (27, 28). Understanding the extent to which an aSyn pathology is caused by cell-autonomous as opposed to non–cell-autonomous mechanisms is a fundamental issue when attempting to untangle the events that underpin the progression of these pathologies.

While different animal and cellular models recapitulate different aspects of aSyn pathology, such as aggregation or phosphorylation, they do not allow the relevance of such features to be linked to neuronal survival. To address this limitation, we previously developed an automated microscopy method to track individual neurons expressing fluorescently tagged neurotoxic proteins over long periods of time. Longitudinal tracking of individual neurons enables the risk of neuronal death to be determined quantitatively and Cox regression models to be applied to evaluate predictive factors of neuronal death (29–33). Given the relevance of neurotoxic protein dynamics in neurodegeneration, this approach was then adapted to determine the protein's half-life in individual living neurons (optical pulse labeling, OPL) (34, 35). Based on this approach, we have now developed a neuronal model to assess the risk of death when neurons express WT or mutant aSyn alleles. We then investigated whether the main hallmarks of aSyn pathology, such as protein stability, aggregation, or S129 phosphorylation, contribute to neuronal death. Finally, we developed an assay to quantitatively assess whether aSyn toxicity occurs in a cell-autonomous or a non–cell-autonomous manner, based on the capacity of aSyn-expressing neurons to affect the survival of surrounding cells.

Results

The E46K aSyn Pathological Mutation Is the Most Toxic Mutation in Primary Cultures of Rat Cortical Neurons. To identify and track aSyn-expressing neurons over time, we generated WT and pathological aSyn alleles (A30P, E46K, and A53T) fused to monomeric Cherry (Ch) fluorescent protein. The fusions were inserted at the C terminus to avoid interference with any aSyn N-terminal posttranslational modifications (36). Individual rat cortical primary neurons transfected with plasmids encoding Ch-tagged WT or mutant aSyn versions (SynCh, A30PSynCh, E46KSynCh, and A53TSynCh) and the Ch protein alone as a control were subjected to longitudinal tracking by automated microscopy and survival analysis (Fig. 1A). Both fluorescence intensity (as a surrogate measure for protein expression) (Fig. S1) and survival time (the last time each neuron was observed alive) were estimated for individual neurons. A Cox proportional hazard (CPH) analysis indicated that the WT and mutant (A53T and E46K) aSyn significantly increased the risk of death with respect to control (Ch) neurons. The E46K mutant was the most toxic construct (Fig. 1B) based on the hazard ratio (HR) coefficients for each of the aSyn constructs relative to the control (Ch): E46KSynCh, HR 1.82, $P < 0.001$, 95% CI 1.6–2.1; A53TSynCh, HR 1.36, $P < 0.001$, 95% CI 1.2–1.6; SynCh, HR 1.22, $P < 0.01$, 95% CI 1.1–1.4; A30PSynCh, HR 1.1, $P = 0.46$, 95% CI 0.9–1.3. The similar steady-state protein levels of all aSyn variants tested ruled out any differences in protein
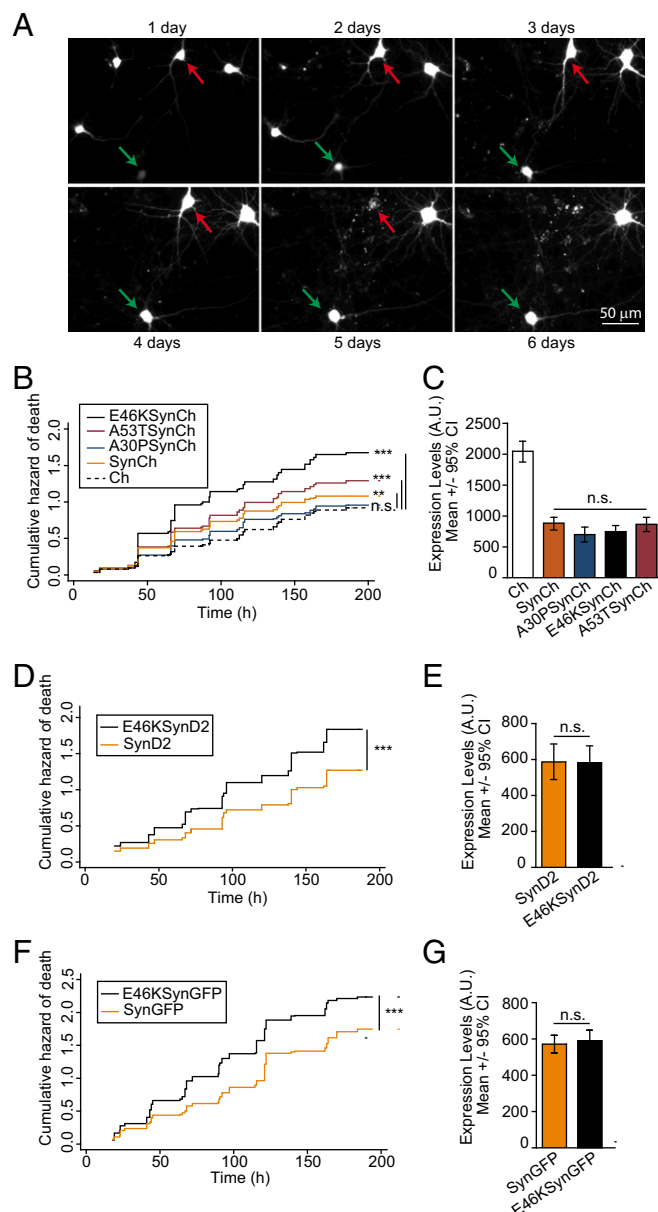

Fig. 1. The E46K aSyn mutant significantly increases the risk of neuronal death in primary cultures of rat cortical neurons. (A) Longitudinal tracking with automated microscopy of individual primary rat cortical neurons transiently transfected with Ch. The green arrow points to a neuron tracked longitudinally for up to 6 dpt; the red arrow indicates a neuron that died 5 dpt. (B) Cumulative hazard estimates of primary neurons transfected with WT aSyn (SynCh), with the pathological mutants A30PSynCh, E46KSynCh, or A53TSynCh, or with Ch as control. Results show CPH analysis of 500–750 neurons per condition from four independent experiments. (C) Ch fluorescence intensity of individual neurons 20–24 h after transfection ($n = 80$–160 neurons per condition from a representative experiment; Kruskal–Wallis and Dunn's post hoc test). (D and F) Cumulative hazard estimates of primary neurons transfected with D2/GFP-tagged WT aSyn or the E46K mutant (SynD2, SynGFP, E46KSynD2, E46KSynGFP). CPH analysis: D2 fusions, $n =$ around 500 neurons per condition from four independent experiments; GFP fusions, $n =$ around 900 neurons per condition from five independent experiments. (E and G) Expression of aSyn (WT or E46K mutant) in neurons at 20–24 h after transfection ($n =$ around 100 neurons per condition from representative experiments Mann–Whitney test). All error bars indicate 95% CIs; n.s., nonsignificant; **$P < 0.01$; ***$P < 0.001$.

abundance underlying the distinct toxicity observed among the aSyn alleles (Fig. 1*C*). Moreover, similar results were obtained when using monomeric GFP- or Dendra2 (D2)-tagged constructs (Fig. 1 *D–G*): E46KSynCh versus SynCh, HR 1.46, *P* < 0.001, 95% CI 1.35–1.58; E46KSynD2 versus SynD2, HR 1.39, *P* < 0.001, 95% CI 1.2–1.6; E46KSynGFP versus SynGFP, HR 1.35, *P* < 0.001, 95% CI 1.2–1.5. Notably, the different fluorescent tags used in this study produced different levels of background toxicity (Table S1 and Fig. S2*A*), and therefore the intrinsic D2 and GFP toxicity masked the WT aSyn toxicity (Fig. S2 *C* and *E*). To rule out the possibility that tagging could affect aSyn behavior/toxicity, we tested the toxicity of untagged aSyn versions expressed from a dicistronic mRNA, which expresses GFP in an internal ribosome entry site (IRES)-dependent manner. Since IRES-driven GFP fluorescence was not sufficient to identify and track transfected neurons, un-tagged constructs (pCAGGs-Syn-IRES-GFP or pCAGGs-E46KSyn-IRES-GFP) were cotransfected with Ch (Fig. S3). Similar toxicity levels were found between untagged and tagged aSyn versions (Fig. S3 *A* and *B*). Taken together, our analyses identify E46K aSyn as the most toxic pathological mutation.

The E46K Mutation Does Not Affect Either aSyn Protein Turnover (Half-Life) or Its Propensity to Aggregate. A possible explanation for the contribution of pathological aSyn mutations to neuro-degeneration is that aSyn mutations may interfere with protein-degradation pathways (12, 37), thereby increasing aSyn concentrations and toxicity. Alternatively, the aSyn mutations may favor the adoption of more toxic, aggregation-prone protein confor-mations (13). Thus, we investigated whether E46K-dependent toxicity was associated with altered protein stability and/or degra-dation. We performed OPL experiments to estimate protein turn-over (half-life) in primary neurons in vivo (34, 35). The OPL approach overcomes the need for radioactivity and the use of translational inhibitors in conventional protocols, and it enables protein stability to be studied in individual neurons. OPL experiments are based on the biophysical properties of the fluorescent protein D2 (38), a photoconvertible fluorescent protein that normally emits green fluorescence but that changes its conformation irreversibly upon an intense pulse with blue light, emitting red fluorescence. The photoconverted protein pool can be tracked over time in vivo using automated longitudinal microscopy, such that the red fluorescence intensity (RFI) will decline over time due to protein turnover (Fig. 2*A*). RFI decays following an exponential pattern in individual neurons (Fig. 2*B*). Thus, logarithmic transformation of RFI measurements for each individual neuron and further adjustment by linear regression enables the D2 half-life in indi-vidual neurons to be determined from the slope (K): $t_{1/2} = -\ln(2)/K$ (Fig. 2*C*).

The stability of D2-tagged WT and mutant aSyn alleles ex-pressed in primary cortical neurons was assessed by OPL. The half-life of WT aSyn was previously estimated to be around 50 h in nonneuronal and neuronal cell lines (7, 39). As such, images were obtained every 12 h after photoconversion over a total of ≈160 h. In the majority of neurons (around 95%) the decay of WT or mutant aSyn-D2 protein followed exponential decay ki-netics, such that the half-life was estimated only in neurons with a coefficient of R^2 >0.7. Accordingly, we found the half-life of WT aSyn in primary neurons to be ≈47 h. In contrast to earlier reports (12), we did not observe a longer half-life for the A53T or A30P aSyn mutants compared with the WT (Fig. 2*D*). More-over, and despite its higher toxicity, the E46K mutation did not affect aSyn protein turnover. Similar results were obtained when only neurons with a coefficient of determination R^2 >0.9 were an-alyzed (≈78% of the total neurons) (Fig. 2*E*). Notably, the esti-mated half-life in these experiments did not depend on the initial amount of photoswitched protein (initial RFI, RFI_0) (Fig. 2*F*). Thus, the toxicity observed with E46K mutation was not due to an increase in protein stability.

We investigated whether E46K toxicity resulted from enhanced abnormal aggregation, based on the formation of round, bright puncta in neurons expressing fluorescently tagged toxic proteins
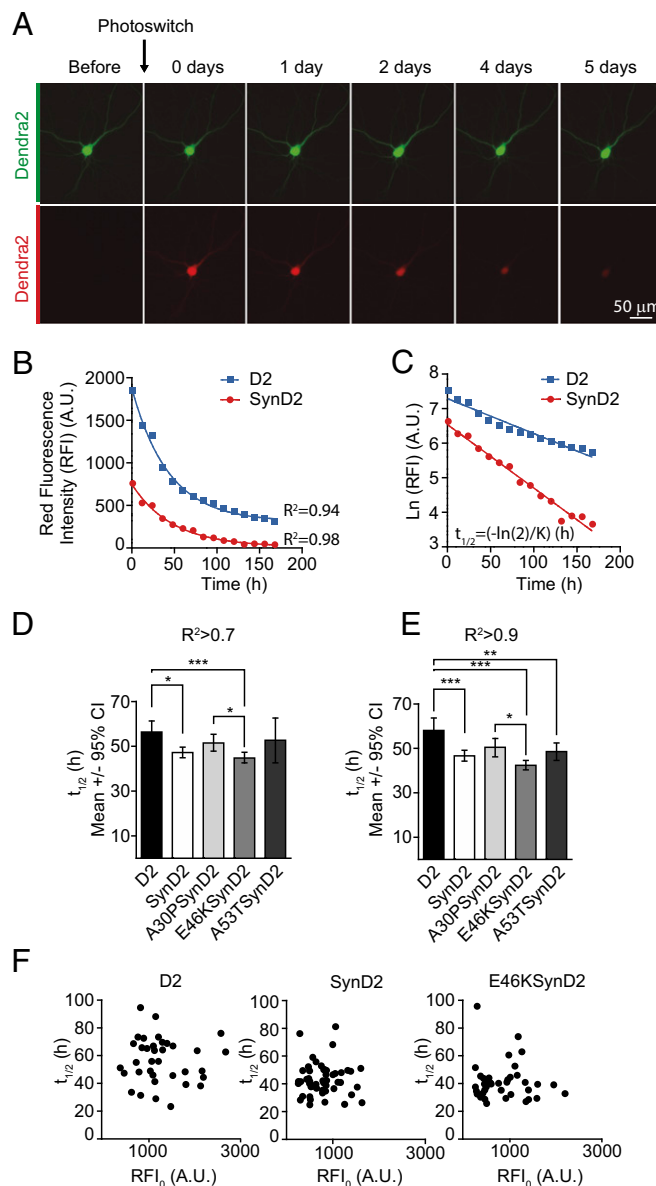

Fig. 2. The E46K mutation does not alter aSyn protein stability. (*A*) Protein turnover (half-life) estimated in living neurons by OPL. (*Upper Row*) Illumi-nation of a D2-transfected neuron with light at a wavelength of 488 nm induces the emission of green fluorescence. (*Lower Row*) After a brief pulse with intense blue light (photoswitching), a proportion of the D2 molecules photoconvert and emit red fluorescence. Green and red fluorescence in-tensities in single neurons are longitudinally monitored by automated mi-croscopy. (*B*) Example of two photoconverted neurons in which changes in RFI over time fit an exponential decay. (*C*) Logarithmic transformation of the intensity of RFI [ln(RFI)] and adjustment by linear regression. The slope (K) enables the D2 half-life to be estimated ($t_{1/2} = -\ln(2)/K$) in individual neu-rons in hours (h). (*D* and *E*) Half-life estimated for D2-tagged WT aSyn (SynD2) and pathological mutants A30PSynD2, E46KSynD2, and A53TSynD2 in neurons subjected to OPL. Graphs show the estimated half-life for neurons with coefficients of determination R^2 >0.7 (*D*) and R^2 >0.9 (*E*) (Kruskal–Wallis and Dunn's post hoc test, *n* = 130–290 neurons per condition from five independent experiments). (*F*) No correlation was found between the initial RFI after pho-toconversion (RFI_0) and the protein half-life estimated in individual neurons transfected with D2 or D2 aSyn-tagged constructs (*n* = 30–50 neurons per con-dition, a representative experiment). All error bars indicate 95% CIs; *P < 0.05, **P < 0.01, ***P < 0.001.

(e.g., mutant huntingtin) constituting visual proof of aggregation (30, 32, 33, 35). Visual inspection of cortical primary neurons transfected with WT or E46K aSyn revealed that aSyn was distributed homogeneously, and the formation of aggregates was not apparent during the experiments (see representative images in Fig. 3A). Since aSyn aggregates are resistant to extraction with nonionic detergents such as 1% Triton X-100 (1% Tx-100) (40), we performed detergent-extraction experiments to assess whether E46K aSyn had a greater propensity to form aggregates. We infected primary cortical neurons with lentiviruses expressing WT or E46K together with an IRES-driven GFP reporter (41). Compared with transient transfection experiments, lentiviral transduction yielded lower aSyn levels in individual neurons and recapitulated E46K and WT aSyn toxicity (Fig. S3 E and F). Since our longitudinal survival experiments were carried out for up to 8 d, extracts of the primary neuronal cultures were prepared 5 and 10 d after lentiviral infection by homogenization in buffer con-

taining 1% Tx-100, and the Tx-100–soluble and –insoluble protein fractions were analyzed by Western blots. If aggregate formation occurs, aSyn should appear in the insoluble protein fraction, but both WT and E46K aSyn were found predominantly in the Tx-100–soluble fraction at 5 and 10 d after infection, with a mass of ≈16 kDa (Fig. 3B and Fig. S4). As controls for correct extract fractionation, tubulin appeared in the soluble fraction and vimentin in the insoluble fraction (42). Thus, E46K toxicity cannot be explained by changes in aSyn stability or aggregation. Indeed, our model recapitulates the induction of E46K aSyn-dependent neuronal toxicity before insoluble aggregates appear. Accordingly, we postulate that soluble aSyn species may act as toxicity drivers and that aggregation may take place at later stages of neurodegeneration.

E46K Toxicity Correlates with Strong PLK2-Dependent S129 Phosphorylation, but Phosphorylation Does Not Explain E46K Toxicity. Posttranslational modifications such as S129 phosphorylation (PS129) could play a role in aSyn toxicity (14), and thus we measured the PS129 in neurons expressing the WT or mutant forms of aSyn by immunofluorescence using a PS129-specific antibody. The pathological mutation E46K exhibited the highest levels of PS129 (Fig. 4 A–C and Figs. S3C and S5 A–C), confirming recent data (43). Moreover, the extent of PS129 correlated with the degree of aSyn toxicity (Fig. 1B).

Two kinases, Polo-like kinase 2 (PLK2) and G protein-coupled receptor kinase 5 (GRK5), have been shown to phosphorylate S129 in neurons (44, 45). To assess the contribution of these two kinases to aSyn PS129 in our neuronal model, we cotransfected aSyn with plasmids encoding validated shRNAs against rat PLK2 (46, 47) or human/rat GRK5 (Fig. S5D) (48). Although both shRNAs seemed to reduce the PS129 of the WT and E46K aSyn, only PLK2 silencing yielded a significant inhibition (around 85% reduction) (Fig. 4 D–F and Fig. S5E). Indeed, a selective PLK2 inhibitor (49) inhibited PS129 in a dose-dependent manner, an effect that was observed 48 h after inhibition and that persisted for up to 8 d at the higher doses (Fig. 4G). By contrast, the GRK5 inhibitor amlexanox (50) did not diminish the PS129 aSyn (Fig. 4H), suggesting that PLK2 was the major driver of neuronal aSyn PS129.

Whether aSyn PS129 is causally related to neuronal death remains under debate. Given the close correlation between PS129 levels and aSyn-dependent toxicity, we tested whether PS129 contributes to neuronal death by inhibiting PLK2-dependent aSyn phosphorylation and by generating phosphorylation-incompetent aSyn mutants (S129A). In longitudinal survival analyses of primary cortical neurons cotransfected with E46K aSyn and PLK2 shRNAs, the PLK2 shRNAs decreased PS129, but they did not alter aSyn E46K-dependent toxicity (the increased toxicity with sh1PLK2 was probably due to off-target effects) (Fig. 5 A and B). As a complementary approach, we evaluated the effect of pharmacological inhibition of PLK2 on the survival of E46KSynD2–overexpressing neurons. Again, while the PLK2 inhibitor produced a decrease in aSyn PS129 (Fig. 4G), no changes in neuronal death were evident (Fig. 5C). Furthermore, longitudinal survival analysis of neurons expressing WT or mutant aSyn (E46K, S129A, or E46KS129A) demonstrated that blocking PS129 did not reduce E46K-dependent neuronal toxicity (Fig. 5D and Fig. S5F).

Together, these results confirm PS129 to be a pathological hallmark of aSyn-dependent neurodegeneration and identify PLK2 as a major driver of this phosphorylation. However, as the turnover or aggregation of the heavily phosphorylated E46K protein was not altered in our experimental model, PLK2-dependent aSyn phosphorylation would appear to precede the formation of LBs, and as such it may represent an effective biomarker for early alterations in PD. Nevertheless, our results demonstrate that aSyn PS129 does not explain the toxicity of this protein, and they suggest that this pathological hallmark could be an epiphenomenon.

E46K Toxicity Is Predominantly Cell Autonomous. Since our experimental approach documents the death of neurons overexpressing WT or mutant aSyn, and particularly the E46K mutation, it is
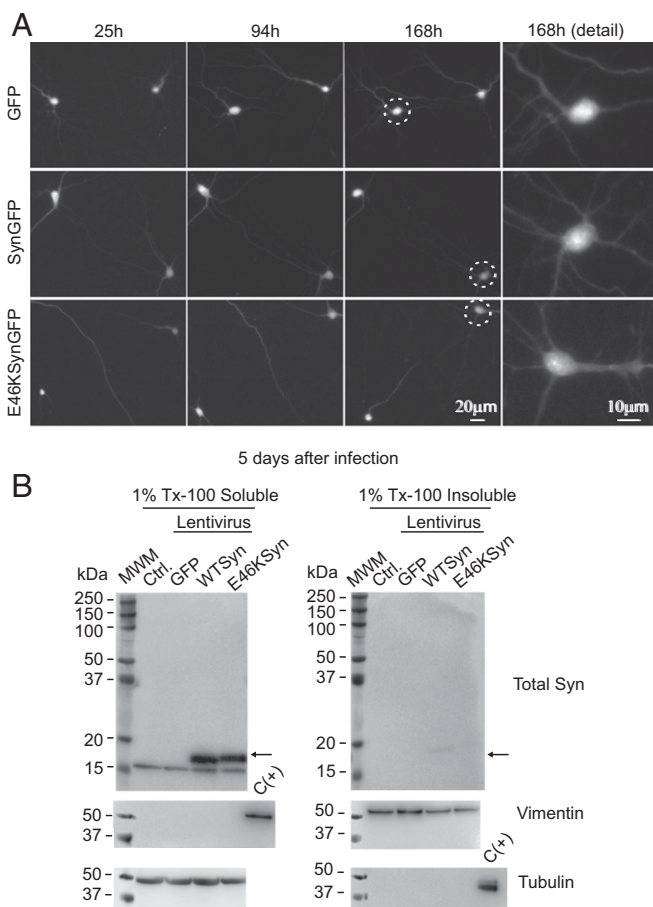

Fig. 3. The E46K mutant does not form Tx-100–insoluble aggregates in rat primary cortical neurons during a longitudinal survival experiment. (A) Visual inspection does not reveal aggregate formation in neurons transfected with GFP, SynGFP, or E46KSynGFP. The circles show neurons that are amplified in the image at the *Right*. (B) Rat cortical primary neurons were infected with lentivirus expressing aSyn (WT or E46K mutant) together with an IRES-driven GFP reporter (41), and 5 d after lentiviral infection the primary neuronal cultures were extracted with 1% Tx-100. The detergent-soluble and -insoluble protein fractions were separated by ultracentrifugation and analyzed by Western blots. As reported elsewhere (42), tubulin appears in the soluble fraction and vimentin in the insoluble fraction. A sample from the opposite fraction was used as a positive control [C(+)]. The aSyn from these cells is predominantly detected in the 1% Tx-100–soluble fraction, with a mass of ≈16 kDa. Experiments were performed twice with similar results. Ctrl, control noninfected neurons; MWM, molecular weight marker.
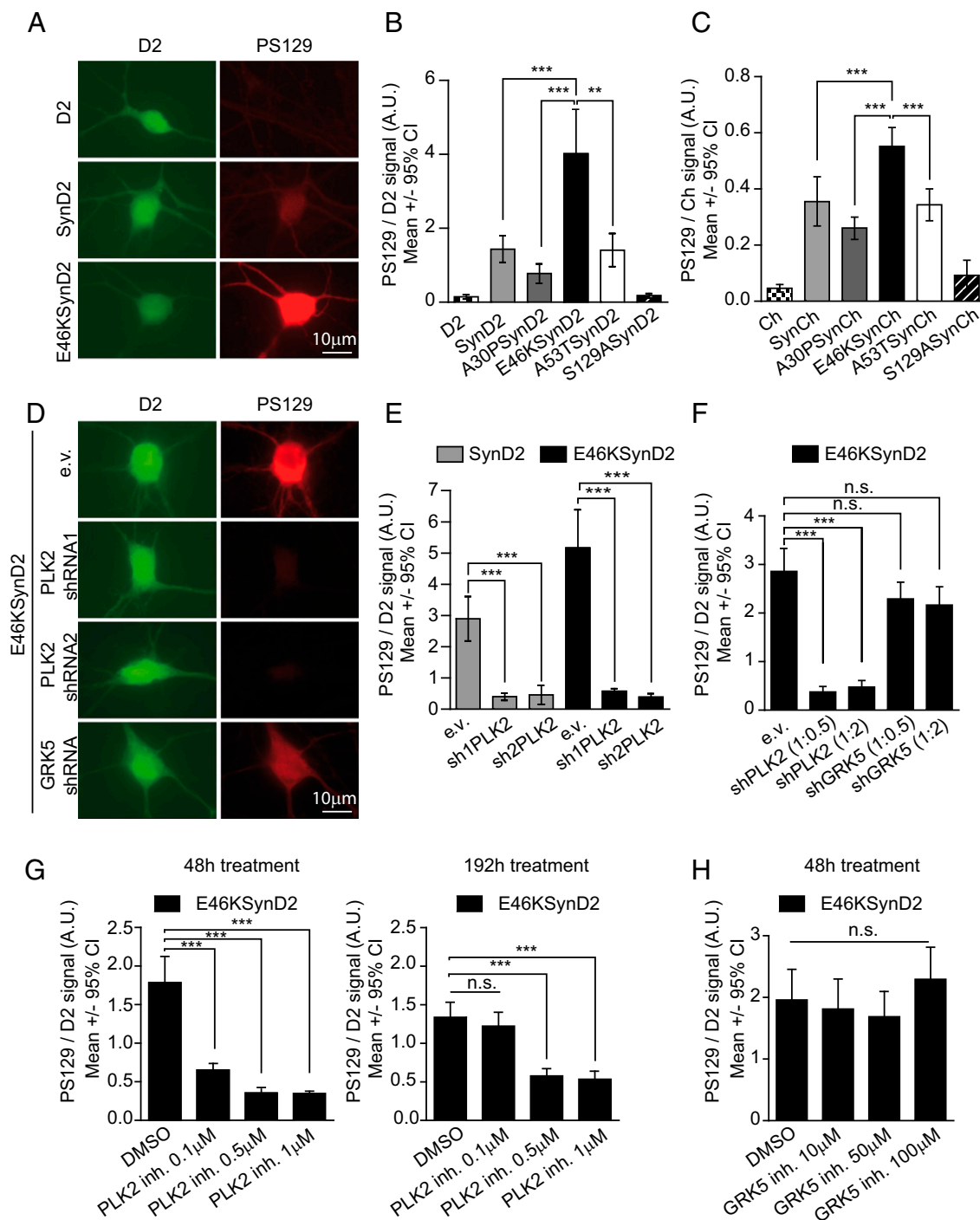
Fig. 4. The E46K mutant exhibits the highest levels of PLK2-dependent PS129. (*A*) Immunofluorescence staining of primary rat cortical neurons expressing D2 or E46KSynD2 with a specific antibody against PS129. The green fluorescence signal from D2 is a surrogate for total aSyn levels, and the red fluorescence signal indicates the anti-PS129 binding (PS129 levels). (*B*) Quantification of the anti-PS129 binding over the D2 fluorescence intensity (total aSyn) in individual neurons expressing SynD2, A30PSynD2, E46KSynD2, or A53TSynD2; neurons expressing D2 and the S129ASynD2 mutant were used as negative controls (*n* = 20–40 neurons per condition; results of a representative experiment of three independent experiments are shown). (*C*) Similar results were obtained for aSyn Ch-tagged versions (*n* = around 30 neurons per condition). (*D*) Neurons cotransfected with E46KSynD2 and PLK2/GRK5 shRNAs containing plasmids or the empty vector (e.v.) as a control and immunostained with the anti-PS129 antibody. (*E*) Quantification of anti-PS129 binding relative to the D2 fluorescence intensity (total aSyn) in individual neurons expressing SynD2 or E46KSynD2 with two specific PLK2 shRNAs, sh1PLK2 and sh2PLK2. (*n* = 8–23 neurons per condition; results of a representative experiment of at least four independent experiments are shown). (*F*) Anti-PS129 binding relative to the D2 fluorescence intensity (total aSyn) in individual neurons expressing E46KSynD2 with PLK2- and GRK5-specific shRNAs at ratios of 1:2 and 1:0.5 (*n* = 30–44 neurons per condition from two independent experiments). (*G*) Quantification of PS129 in neurons expressing E46KSynD2 48 and 192 h after addition of the PLK2-specific inhibitor (inh). The effect persists at the higher doses 192 h after addition (*n* = 30–35 neurons per condition; results from a representative experiment of at least two independent experiments are shown). (*H*) A similar experiment using a GRK5-specific inhibitor did not decrease PS129 after 48 h (*n* = 20 neurons; results from a representative experiment of two independent experiments are shown). All error bars indicate 95% CIs; n.s., nonsignificant; **$P < 0.01$, ***$P < 0.001$ Kruskal–Wallis and Dunn's post hoc test.
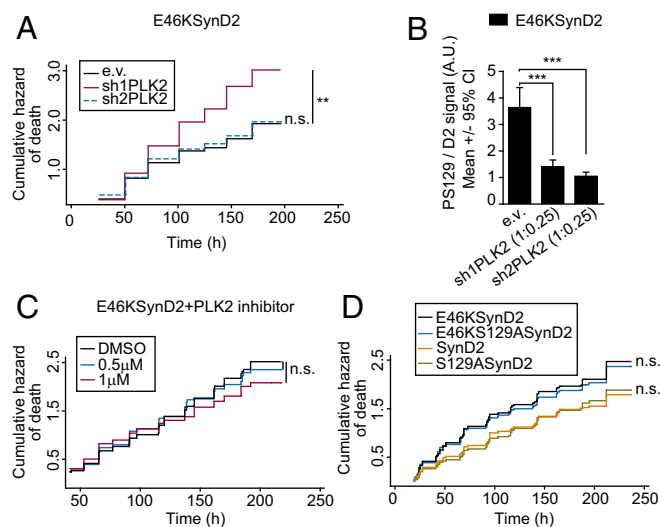
Fig. 5. PLK2-dependent PS129 does not explain the E46K-dependent toxicity. (*A*) Cumulative hazard estimates of primary rat cortical neurons coexpressing E46KSynD2 and PLK2 shRNAs (sh1PLK2 and sh2PLK2) (log-rank test; n = around 150 neurons per condition). (*B*) Quantification of PS129 relative to the D2 fluorescence intensity (total aSyn) by immunostaining individual neurons expressing E46KSynD2 and PLK2 shRNAs with the specific anti-PS129 antibody. Under the same conditions used in *A*, PLK2 shRNAs significantly reduced E46KSynD2 PS129 (Kruskal–Wallis and Dunn's post hoc test; n = 18–26 neurons per condition). (*C*) Neurons transiently transfected with E46KSynD2 were treated with two doses of the PLK2 inhibitor previously tested and subjected to longitudinal survival analysis (log-rank test; n = 600–1,000 neurons from five independent experiments). (*D*) Longitudinal survival of neurons expressing aSyn WT or the pathological E46K mutation $\pm$ the S129A mutation (CPH analysis; n = 2,500 neurons per condition from seven independent experiments). All error bars indicate 95% CIs; n.s., nonsignificant, **P < 0.01, ***P < 0.001.

tempting to assume a priori that toxicity occurs in a cell-autonomous manner. However, aSyn protein could propagate from neuron to neuron in distinct complexes (e.g., monomers, oligomers, or aggregates), spreading toxicity through a non–cell-autonomous mechanism. In addition to the mobilization of aSyn species from cell to cell, E46K toxicity could propagate to neighboring neurons by other means, such as through the release of cell debris after neuronal death or through changes in neuronal activity. For instance, overexpression of the E46K mutant in hippocampal neurons inhibits neurotransmitter release (51).

To establish the contribution of non–cell-autonomous mechanisms to aSyn toxicity, we developed an experimental set-up to measure whether neurons expressing a toxic protein affect their neighbors' risk dying. Primary cortical neurons were transfected first with a plasmid expressing a control GFP protein and 24 h later with a second plasmid expressing the Ch-tagged toxic protein of interest. As the probability of cotransfected neurons is very low (around 0.2–0.3% of neurons), the resulting culture contains two different neuronal populations: control neurons expressing GFP (in green) and toxic neurons expressing Ch-tagged toxic proteins (in red) (Fig. 6*A*). This allows the risk of death of control neurons when surrounded by neurons expressing neurotoxic proteins to be scored. We acquired adjacent nonoverlapping fields of these neuronal cultures covering a total area of around 46 mm² and combined them to create a single tiled image (Fig. 6*A*). "Green" and "red" neurons were tracked by automated microscopy for up to 8–9 d, and we estimated the individual survival time and assigned relative positions (*x/y* coordinates) for each individual neuron in the tiled image.

To validate the approach, we overexpressed an established inducer of nonautonomous toxicity, mutant human amyloid precursor protein (APP). In Alzheimer disease (AD), abnormal APP leads to the accumulation of amyloid-β (Aβ) extracellular aggregates that impair synaptic function and trigger neuronal loss (52). Pathological APP mutations increase both the amount and aggregation propensity of Aβ peptides. Extracellular Aβ secreted by neurons expressing APP harboring the Swedish and London mutations (APPswe/lnd) impairs long-term potentiation of adjacent neurons that do not express APPswe/lnd (53). We transfected primary cortical neurons with GFP (as a control) followed by cotransfection with constructs expressing the APPswe/lnd mutant (53) and Ch (APP+Ch). Taking advantage of the strong correlation between APP and Ch expression (Fig. 7 *A* and *B*), we used red fluorescence as a surrogate for APP expression. The risk of death for APP+Ch-expressing neurons was estimated by a CPH analysis, and, as expected, neurons expressing APPswe/lnd had a high risk of death, increasing at higher doses (*hd*) of the APP plasmid (APP+Ch HR, 1.65; APP*hd*+Ch HR, 2.46) (Table 1). We then scored the risk of death of control GFP neurons neighboring APP+Ch neurons; higher doses of APP significantly affected the survival of control cells [GFP(APP*hd*+Ch) HR 1.31] (Table 1). The risk of death increased during the experiment, such that a significant risk of death could only be detected at the later time points (Fig. 7*C*). Hence, a CPH analysis was performed considering the variable group as a time-varying covariate (tvc), which confirmed that the relative hazard of GFP neurons cocultured with (APP*hd*+Ch)-expressing neurons changed over time, following the equation: HR = 0.76 × (1.01)^t (Table S2). The effect of (APP*hd*+Ch)-expressing neurons over GFP control neurons starts to be significant 100 h after transfection (Fig. 7*D*). Therefore, our experimental set-up is sensitive to detect non–cell-autonomous toxicity in neurons.

We next evaluated whether neurons overexpressing Ch-tagged WT and E46K aSyn could influence the survival of neighboring GFP-expressing neurons. WT and E46K aSyn overexpression significantly increased the risk of neuronal death (SynCh HR = 1.33 and E46KSynCh HR = 1.94) (Table 2). However, neither GFP neurons that neighbored SynCh-expressing neurons nor GFP neurons neighboring E46KSynCh-expressing neurons experienced a significant increase in the risk of death compared with control conditions (GFP neurons neighboring Ch-expressing neurons) (Table 2).

The previous experiments analyzed the nonautonomous toxicity in a manner independent of distance (i.e., the effect comes from the whole set of neurons within the tiled image). Nevertheless, nonautonomous toxicity could be further modeled as a function of the number of neurons that are located in close vicinity and express a neurotoxic factor. If that were the case, the proximity and number of neurons expressing a neurotoxic protein would affect the risk of death of control neurons. Taking this possibility into account, we defined the variable, n_r, that accounts for the number of neurons expressing a neurotoxic protein (SynCh or E46KSynCh), or Ch as a control, within a circle of radius (r) centered on each GFP$^+$ control neuron (Fig. 6 *B* and *C*). The radii of r = 500 μm and r = 1,000 μm were investigated based on the frequency distribution of n_r for the whole set of GFP neurons in the tiled image (Fig. S6). Subsequently, we estimated the risk of death of GFP$^+$ neurons by using CPH models adjusted to n_r (Table 3 and Table S3). In the adjusted model (with the group and n_r factors), the group factor (SynCh or E46KSynCh) did not show any effect on the risk of death of neighboring GFP$^+$ neurons (compared with neighboring Ch neurons). On the other hand, n_r did have a significant influence on this parameter (Table 3). Interestingly, a significant interaction between the group and n_r factors was evident for both r = 500 μm and r = 1,000 μm (Wald test, P < 0.001). In particular, we found a small but significant effect on the risk of death of GFP neurons neighboring E46KSynCh neurons (HR 1.03 for r = 500 μm and HR 1.01 for r = 1,000 μm) but not for the GFP neurons neighboring SynCh neurons (Table 3 and Table S3). Hence, this mild nonautonomous effect observed in our E46KSynCh primary cultures appeared to decrease over distance and escapes the detection threshold at the whole-population level. Of note, further microscopy analysis gave no evidence of cell-to-cell spread of E46K aSyn species to GFP control neurons (Fig. S7) that could explain this mild nonautonomous effect.
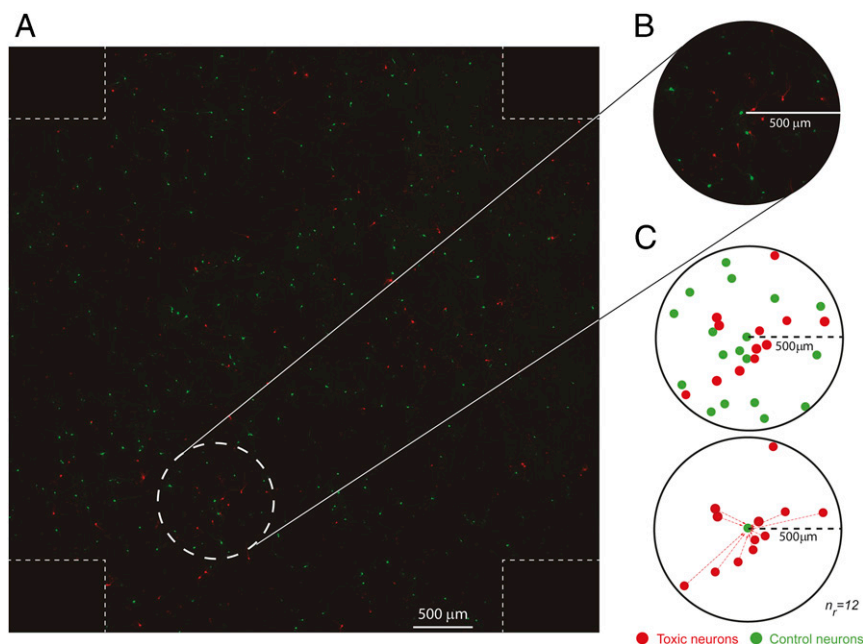
Fig. 6. Experimental strategy to study the contribution of non–cell-autonomous mechanisms in neuronal death. (*A*) To assess the potential contribution of non–cell-autonomous mechanisms to neuronal death, we assessed how the risk of death in neurons expressing a control protein (i.e., GFP) is influenced by neighboring neurons expressing a toxic protein (i.e., Ch-tagged aSyn constructs). To that goal, we longitudinally imaged primary rat cortical neurons transiently transfected with control and toxic proteins in the same field. Shown is an example of a single tiled image of these neurons created with adjacent nonoverlapping images. Individual survival times were estimated for each individual neuron, and a CPH analysis was used to analyze how toxic neurons (red) influenced the risk of death of control neurons (green). (*B*) Magnified image of the area within the dashed circle in *A* showing toxic and control neurons within a 500-μm radius. (*C*) The number of toxic and control neurons within a 500-μm radius around a single control neuron. The number of red (toxic) neurons in a particular radius around each single GFP (control) neuron is the variable n_r (in the example, $n_r = 12$). The n_r was calculated for each single GFP neuron in the tiled image at radii of 500 μm and 1,000 μm.

Therefore, and although we were able to identify a minor non-autonomous component that was spatially restricted, E46K aSyn toxicity is predominantly cell autonomous.

Discussion

We describe here an in vitro neuronal model that recapitulates aSyn toxicity based on the expression of fluorescently tagged aSyn in primary cultures of rat cortical neurons (WT and the pathological A30P, E46K, and A53T mutants), coupled to the longitudinal tracking of individual neurons over a protracted time course by automated microscopy. Our experimental set-up enables a longitudinal survival analysis to be applied, yielding quantitative estimations of the risk of neuronal death associated with aSyn and allowing its toxicity to be investigated. Through this approach, we were able to identify the pathological E46K aSyn mutation as the most toxic variant, although its enhanced toxicity was not due to enhanced protein stability or aggregation, and it was triggered by soluble aSyn species. We also found that a main pathological feature of PD, S129 aSyn phosphorylation, was strongly correlated with aSyn toxicity, such that the strongest PS129 was associated with the E46K mutation. PLK2 was identified as the main S129 kinase in neurons, but independent approaches demonstrated that PS129 does not play a causative role in neurotoxicity and that, instead, it probably represents an epiphenomenon. Nevertheless, the strong correlation between PS129 and the risk of neuronal death suggests that it could be a useful biomarker for early disease stages. Finally, we evaluated whether E46K-expressing neurons confer susceptibility to death to neighboring control neurons. While we identified a minor E46K-dependent nonautonomous toxic component, it was spatially restricted to local neighbors. Thus, in our experimental set-up E46K aSyn toxicity is predominantly due to cell-autonomous mechanisms.

Patients with mutations in the *SNCA* gene often display cognitive impairment (54), which appears to be strongly associated with the E46K mutation. Indeed, the patients in which this mutation was first described developed severe cognitive decline, dementia, and visual hallucinations, all features associated with DLB (55). This is consistent with our results showing E46K to be the most toxic mutation in cortical neurons. We also found that the A53T mutation decreases neuronal survival, albeit to a lesser extent than the E46K mutation. Notably, the toxicity associated with WT aSyn reached statistical significance only with Ch-tagged versions, probably because of the low intrinsic toxicity that this fluorescent protein displays. Toxicity of D2-tagged WT aSyn was reported recently, but differences in the expression vector used or the fact that fusions were performed N-terminally could account for this discrepancy (35).

The toxicity evident in our in vitro system (E46K > A53T > WT) has been observed in mouse models in which aSyn variants are overexpressed in the substantia nigra by lentiviral transduction (41). Intriguingly, our results did not recapitulate the A30P-associated toxicity, a mutant that stands apart from the other mutants in different experimental assays. For instance, A30P aSyn has the slowest propensity to induce fibril formation in vitro (56), and it is equally or less toxic than WT aSyn in yeast models (57). It is noteworthy that the A30P mutation disrupts the membrane association of aSyn (58). Indeed, overexpression of WT, E46K, and A53T aSyn in hippocampal primary neurons inhibits synaptic vesicle exocytosis and neurotransmitter release, while the A30P mutant does not (51). Given these differences, it is reasonable to assume that the mechanism of A30P toxicity could differ from that of the other aSyn mutants.

Compared with animal models of aSyn toxicity, the primary culture model described here recapitulates neuronal loss. Overexpression of human E46K aSyn in rodents reproduces motor impairment and the formation of aSyn intraneuronal aggregates resembling LBs, but neuronal death was not reported (59, 60). Similarly, most WT and mutant aSyn transgenic mouse models reproduce features of PD, such as striatal dopamine loss, aSyn aggregation, and/or motor impairment, but not neuronal death in the substantia nigra (61). Nevertheless, neuronal death has been reported in a conditional murine model expressing WT and A30P aSyn and in a BAC model
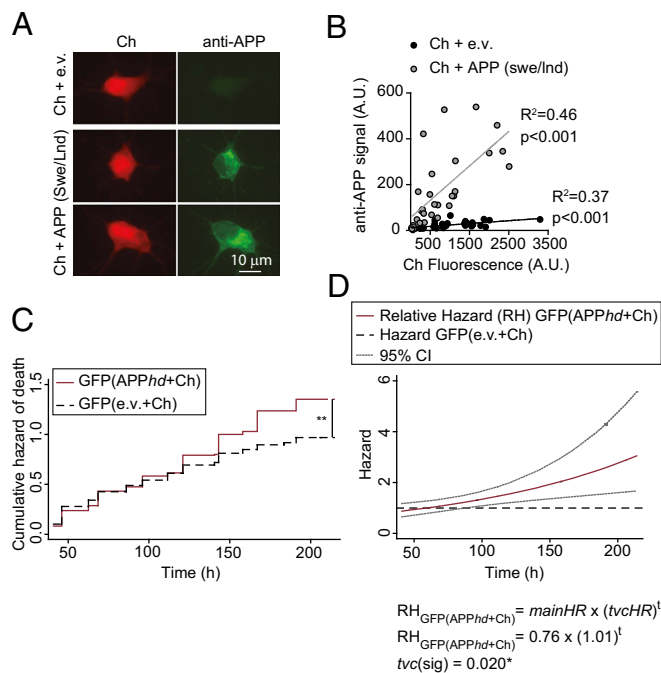
Fig. 7. Neurons expressing APPswe/Lnd increase the risk of death of neighboring control neurons. (*A*) Primary rat cortical neurons were cotransfected with plasmids expressing APPswe/lnd or the empty vector (e.v.) and Ch and were immunostained with an APP-specific antibody. (*B*) Fluorescence intensity from Ch and from secondary antibodies recognizing APP was quantified in individual neurons. A correlation analysis was performed showing that Ch$^+$ neurons expressed the APPswe/lnd protein compared with control conditions (e.v.). (*C*) Cumulative risk estimates of GFP-expressing neurons neighboring APP-expressing neurons transfected with a high dose of APP+Ch (APPhd+Ch) or control neurons (e.v.+Ch). CPH analysis of 250–300 neurons from two independent experiments: **$P <$ 0.01. (*D*) Cox modeling of the time-dependent variation in the relative hazard in a population of neighboring APP-expressing neurons [GFP(APPhd+Ch)] with respect to a population of neighboring control neurons [GFP(e.v.+Ch)]. The main relative hazards at $t = 0$ and tvc are from Table S2 95% CIs.

expressing WT aSyn (62–64). One major advantage of our model is that it recapitulates aSyn-dependent toxicity in a short temporal framework of 8–9 d, and toxicity can be scored quantitatively to explore the molecular mechanisms of aSyn toxicity as well as therapeutic approaches aimed at increasing the survival of neurons.

It has been reported that the pathological A30P and A53T mutations interfere with chaperon-mediated autophagy, thereby altering the degradation of aSyn and other substrates (12). Since increased aSyn steady-state levels are sufficient to promote PD, we determined whether the E46K mutation altered the aSyn half-life in primary living neurons using OPL as an indirect assessment of

Table 1. CPH model of the effect of APPswe/lnd on neuronal survival

Group	HR	95% CI	P value
(APP+Ch) ($n = 838$) vs. (e.v.+Ch) ($n = 812$)	1.65	1.11–2.46	0.014*
(APPhd+Ch) ($n = 643$) vs. (e.v.+Ch) ($n = 703$)	2.46	2.02–2.99	<0.001***
GFP(APP+Ch) ($n = 515$) vs. GFP(e.v+Ch) ($n = 471$)	1.10	0.91–1.33	0.310
GFP(APPhd+Ch) ($n = 294$) vs. GFP(e.v.+Ch) ($n = 254$)	1.31[†]	1.08–1.58	0.006**

n, number of neurons. Data are from three independent experiments.
[†]Violates proportional hazard assumption ($P = 0.013$*).

Table 2. CPH model of the effect of aSyn (WT and mutant E46K) on neuronal survival

Group	HR	95% CI	P value
SynCh ($n = 372$) vs. Ch ($n = 390$)	1.33	1.08–1.64	0.008**
E46KSynCh ($n = 371$) vs. Ch ($n = 390$)	1.94	1.71–2.19	<0.001***
GFP(SynCh) ($n = 581$) vs. GFP(Ch) ($n = 684$)	1.03	0.73–1.44	0.883
GFP(E46KSynCh) ($n = 823$) vs. GFP(Ch) ($n = 684$)	0.96	0.65–1.42	0.851

n, number of neurons. Data are from two independent experiments.

altered degradation. E46K aSyn turnover was similar to that of the WT protein and was even higher than that of A30P aSyn, ruling out altered protein turnover as a driver of E46K toxicity.

Both WT and mutant aSyn concentrate into insoluble oligomers or aggregates of different sizes within neurons, and these species are commonly found in patients and disease models. However, we did not detect overt aggregation in the time course of our experiments, suggesting that protein aggregation is not required for aSyn neurotoxicity. In agreement with this idea, analysis of postmortem human brains affected by synucleinopathies unveiled a dissociation between LBs and neuronal death (65–67). Similar dissociation between aggregation and neuronal death has been reported in experimental models of other neurotoxic proteins [i.e., mutant huntingtin or leucine-rich repeat kinase 2 (LRRK2)] (30, 35) as well as aSyn (64, 68). Thus, our study further supports the notion that aSyn toxicity may arise from early intermediates in the aggregation process (69) or that it is independent of aggregation.

Importantly, we observed differences in aSyn phosphorylation, a pathological hallmark of synucleinopathies, with E46K being the most strongly phosphorylated form, in agreement with recent studies (43). Using specific shRNAs and kinase inhibitors, we identified PLK2 as the kinase preferentially involved in this phosphorylation. PLK2 phosphorylates aSyn S129 in the CNS (44), and it is more concentrated in dopaminergic neurons of aged monkeys (70). The pathological meaning of this posttranslational modification remains unclear. PS129 has been proposed to increase aSyn fibrillization (71) and favor autophagy-dependent aSyn degradation (72), but controversial results have been obtained when trying to link PS129 to neuronal death (15). Our data indicate that PS129 occurs in the absence of aggregation and that it does not alter aSyn turnover (which is even increased in E46K relative to other mutants such as A30P). Here we found a striking correlation between aSyn PS129 and neuronal toxicity, and since PLK2 seems to be the main kinase involved in this modification, we could directly test the contribution of PS129 to neuronal death. Through three independent approaches (modulating PLK2 levels and activity and preventing PS129 with the mutation S129A), we demonstrate that impeding aSyn PS129 does not inhibit neuronal death, indicating that this pathological hallmark is an epiphenomenon. We can hypothesize a scenario in which an increase in PLK2-dependent PS129 coincides with the establishment of toxicity without necessarily contributing to neuronal death. PLK2 is an activity-dependent kinase, the levels of which increase with elevated synaptic activity. In this scenario, PLK2 might phosphorylate substrates involved in rearrangements of the actin cytoskeleton, favoring the spine remodeling that would down-regulate synaptic activity (46, 73). If enhanced aSyn expression leads to changes in neuronal activity, PLK2 could be activated and increase PS129 as part of a program to promote specific substrate degradation and restore neuronal activity. Further experiments should be performed to test this hypothesis.

A growing body of evidence suggests that aSyn species can be released to the extracellular milieu and translocate into neighboring cells by endocytosis. Although the precise mechanism of transmission is not well understood, the hypothesis that aSyn spreading accounts for nonautonomous neuronal death in PD is currently

Table 3. CPH model of the effect of n_r (500-μm radius) on neuronal survival

Variable	HR	95% CI	P value
Group			
GFP(SynCh) ($n = 501$) vs. GFP(Ch) ($n = 590$)	1.09	0.70–1.70	0.694
GFP(E46KSynCh) ($n = 645$) vs. GFP(Ch) ($n = 590$)	0.90	0.57–1.43	0.662
n_r	0.96	0.94–0.99	0.005**
Interaction group # n_r			
GFP(SynCh) ($n = 501$) vs. GFP(Ch) ($n = 590$)	0.99	0.94–1.03	0.576
GFP(E46KSynCh) ($n = 645$) vs. GFP(Ch) ($n = 590$)	1.03	1.00–1.06	0.034*

n, number of neurons; n_r, number of red neurons (Ch, SynCh, E46KSynCh) in a 500-μm radius around each single GFP$^+$ neuron. #, interaction. Data are from two independent experiments.

under debate. While experimental evidence demonstrates that aSyn can promote neuronal death via cell-autonomous and non-autonomous mechanisms, the relative contribution of both mechanisms to toxicity has yet to be established. In our system, E46K aSyn-expressing neurons only marginally influenced the survival of neighboring control neurons, such that only control neurons near E46K aSyn neurons were affected. This effect was largely dependent on the distance and number of toxic neighbors, failing to detect a nonautonomous effect in the whole-population analysis. Although cell-to-cell spread of E46K aSyn could be a tempting explanation for this mild nonautonomous effect, we did not find evidence supporting this notion. By contrast, and as expected, nonautonomous toxicity was detected when APP was overexpressed. This toxicity was time dependent, suggesting that Aβ peptides accumulate in the culture over time. We cannot rule out the possibility that under more toxic regimes, or over longer time scales, nonautonomous E46K toxicity may play a more relevant role. Nevertheless, our results clearly illustrate a more important cell-autonomous component.

Taken together, our model of aSyn toxicity revealed that some of the main hallmarks of aSyn pathology are not necessary to drive neuronal death. We postulate that the cell-autonomous toxicity arising from nonaggregated forms of E46K may recapitulate early events in aSyn toxicity. Among them, PLK2-dependent aSyn phosphorylation could represent an early biomarker of aSyn toxicity that precedes protein aggregation, while the spreading of aSyn through neurons may preferentially occur at later stages of the disease, in the presence of oligomeric species or protein aggregates. Among the aSyn toxic mechanisms proposed, alterations to vesicle trafficking and neurotransmission could underlie E46K toxicity, as well as interference with the endoplasmic reticulum–Golgi transport and the induction of the unfolded protein response (74). Finally, this aSyn neurotoxicity model could serve not only to explain early pathological events of synucleinopathies but also could constitute a platform to assess if new therapeutic approaches enhance the survival of neurons affected by these pathologies.

Materials and Methods

Plasmids. Detailed information on the plasmids used in this study is provided in *SI Materials and Methods*. All plasmids were verified by DNA sequencing.

Neuronal and Cell Cultures, Transfections, and Lentiviral Infections. Animal handling was carried out in accordance with European Community Council Directive 2010/63/EC and Spanish legislation (Real Decreto 53/2013), and the protocols were all approved by the Ethics Committee of the University of Navarra (051-13). Primary cortical neurons were obtained from E20 Sprague–Dawley rat embryos (Charles-River Laboratories). Neurons, HEK293 cells, and McA-RH7777 cells were transfected with Lipofectamine 2000 (Invitrogen) or calcium phosphate after 5 d in vitro. For further details see *SI Materials and Methods*.

Sequential Biochemical Fractionation to Detect Insoluble aSyn Species. Sequential biochemical fractionation of whole-cell lysates from primary cortical neurons (modified from ref. 75) was performed to separate 1% Tx-100–soluble and –insoluble aSyn species. For further details see *SI Materials and Methods*.

Protein Extraction, SDS/PAGE, and Western Blotting. Whole-cell lysates were collected in radioimmunoprecipitation assay (RIPA) buffer 2 d post-transfection (dpt). After protein quantification, the samples were separated by SDS/PAGE and were transferred to nitrocellulose membranes (Bio-Rad Laboratories). The membranes were blocked and then were probed with primary antibodies overnight at 4 °C and with secondary antibodies for 2 h at room temperature (for further details see *SI Materials and Methods*).

Drug Treatments. To evaluate the contribution of the two different kinases to aSyn phosphorylation, two specific kinase inhibitors were applied to the neuronal cultures. Neurons were fixed with a 4% paraformaldehyde (PFA) (Panreac), 4% sucrose (Sigma) solution and visualized by immunofluorescence (for further details see *SI Materials and Methods*).

Immunofluorescence. After fixation with PFA and 4% sucrose, neurons were permeabilized in 0.1% Tx-100, blocked with 3% goat serum (Jackson Immunoresearch) and 3% BSA (Merck-Millipore), and incubated with primary and secondary antibodies for 2 h at room temperature. The coverslips were finally stained with DAPI (Sigma) and observed at 63× magnification on a Zeiss Axiovert 200M fluorescence microscope (for further details see *SI Materials and Methods*).

Automated Image Acquisition. Neuronal survival was studied by automatic longitudinal tracking of neuronal cultures every 12–24 h after transfection on a Zeiss Observer Z1 microscope (29) (for further details see *SI Materials and Methods*).

Image Processing and Statistics. Fluorescence intensity was measured with MetaMorph Analysis software (Molecular Devices), and graphs were generated with GraphPad Prism 5 software. Survival and photoswitching images were analyzed with MATLAB-based custom programs, and survival analysis was performed with STATA 12 (for further details see *SI Materials and Methods*).

Antibodies. Detailed information on the antibodies used in this study is available in *SI Materials and Methods*.

1. Halliday GM, Holton JL, Revesz T, Dickson DW (2011) Neuropathology underlying clinical variability in patients with synucleinopathies. *Acta Neuropathol* 122:187–204.
2. Singleton AB, Farrer MJ, Bonifati V (2013) The genetics of Parkinson's disease: Progress and therapeutic implications. *Mov Disord* 28:14–23.
3. Satake W, et al. (2009) Genome-wide association study identifies common variants at four loci as genetic risk factors for Parkinson's disease. *Nat Genet* 41:1303–1307.
4. Nalls MA, et al.; International Parkinson's Disease Genomics Consortium (IPDGC); Parkinson's Study Group (PSG) Parkinson's Research: The Organized GENetics Initiative (PROGENI); 23andMe; GenePD; NeuroGenetics Research Consortium (NGRC); Hussman Institute of Human Genomics (HIHG); Ashkenazi Jewish Dataset Investigator; Cohorts for Health and Aging Research in Genetic Epidemiology (CHARGE); North American Brain Expression Consortium (NABEC); United Kingdom Brain Expression Consortium (UKBEC); Greek Parkinson's Disease Consortium; Alzheimer Genetic Analysis Group (2014) Large-scale meta-analysis of genome-wide association data identifies six new risk loci for Parkinson's disease. *Nat Genet* 46:989–993.
5. Maraganore DM, et al.; Genetic Epidemiology of Parkinson's Disease (GEO-PD) Consortium (2006) Collaborative analysis of alpha-synuclein gene promoter variability and Parkinson disease. *JAMA* 296:661–670.

6. Soldner F, et al. (2016) Parkinson-associated risk variant in distal enhancer of α-synuclein modulates target gene expression. *Nature* 533:95–99.
7. Theillet FX, et al. (2016) Structural disorder of monomeric α-synuclein persists in mammalian cells. *Nature* 530:45–50.
8. Bartels T, Choi JG, Selkoe DJ (2011) α-Synuclein occurs physiologically as a helically folded tetramer that resists aggregation. *Nature* 477:107–110.
9. Cremades N, et al. (2012) Direct observation of the interconversion of normal and toxic forms of α-synuclein. *Cell* 149:1048–1059.
10. Roberts HL, Brown DR (2015) Seeking a mechanism for the toxicity of oligomeric α-synuclein. *Biomolecules* 5:282–305.
11. Spillantini MG, et al. (1997) Alpha-synuclein in Lewy bodies. *Nature* 388:839–840.
12. Cuervo AM, Stefanis L, Fredenburg R, Lansbury PT, Sulzer D (2004) Impaired degradation of mutant alpha-synuclein by chaperone-mediated autophagy. *Science* 305:1292–1295.
13. Ono K, Ikeda T, Takasaki J, Yamada M (2011) Familial Parkinson disease mutations influence α-synuclein assembly. *Neurobiol Dis* 43:715–724.
14. Fujiwara H, et al. (2002) Alpha-synuclein is phosphorylated in synucleinopathy lesions. *Nat Cell Biol* 4:160–164.
15. Oueslati A (2016) Implication of alpha-synuclein phosphorylation at S129 in synucleinopathies: What have we learned in the last decade? *J Parkinsons Dis* 6:39–51.
16. Brettschneider J, Del Tredici K, Lee VM, Trojanowski JQ (2015) Spreading of pathology in neurodegenerative diseases: A focus on human studies. *Nat Rev Neurosci* 16:109–120.
17. Mollenhauer B, et al. (2012) α-synuclein in human cerebrospinal fluid is principally derived from neurons of the central nervous system. *J Neural Transm (Vienna)* 119:739–746.
18. Tokuda T, et al. (2010) Detection of elevated levels of α-synuclein oligomers in CSF from patients with Parkinson disease. *Neurology* 75:1766–1772.
19. Emmanouilidou E, et al. (2010) Cell-produced alpha-synuclein is secreted in a calcium-dependent manner by exosomes and impacts neuronal survival. *J Neurosci* 30:6838–6851.
20. Danzer KM, et al. (2012) Exosomal cell-to-cell transmission of alpha synuclein oligomers. *Mol Neurodegener* 7:42.
21. Desplats P, et al. (2009) Inclusion formation and neuronal cell death through neuron-to-neuron transmission of alpha-synuclein. *Proc Natl Acad Sci USA* 106:13010–13015.
22. Volpicelli-Daley LA, et al. (2011) Exogenous α-synuclein fibrils induce Lewy body pathology leading to synaptic dysfunction and neuron death. *Neuron* 72:57–71.
23. Luk KC, et al. (2012) Pathological α-synuclein transmission initiates Parkinson-like neurodegeneration in nontransgenic mice. *Science* 338:949–953.
24. Osterberg VR, et al. (2015) Progressive aggregation of alpha-synuclein and selective degeneration of lewy inclusion-bearing neurons in a mouse model of parkinsonism. *Cell Rep* 10:1252–1260.
25. Helwig M, et al. (2016) Brain propagation of transduced α-synuclein involves non-fibrillar protein species and is enhanced in α-synuclein null mice. *Brain* 139:856–870.
26. Braak H, et al. (2003) Staging of brain pathology related to sporadic Parkinson's disease. *Neurobiol Aging* 24:197–211.
27. Walsh DM, Selkoe DJ (2016) A critical appraisal of the pathogenic protein spread hypothesis of neurodegeneration. *Nat Rev Neurosci* 17:251–260.
28. Surmeier DJ, Obeso JA, Halliday GM (2017) Selective neuronal vulnerability in Parkinson disease. *Nat Rev Neurosci* 18:101–113.
29. Arrasate M, Finkbeiner S (2005) Automated microscope system for determining factors that predict neuronal fate. *Proc Natl Acad Sci USA* 102:3840–3845.
30. Arrasate M, Mitra S, Schweitzer ES, Segal MR, Finkbeiner S (2004) Inclusion body formation reduces levels of mutant huntingtin and the risk of neuronal death. *Nature* 431:805–810.
31. Miller J, et al. (2011) Identifying polyglutamine protein species in situ that best predict neurodegeneration. *Nat Chem Biol* 7:925–934.
32. Skibinski G, Nakamura K, Cookson MR, Finkbeiner S (2014) Mutant LRRK2 toxicity in neurons depends on LRRK2 levels and synuclein but not kinase activity or inclusion bodies. *J Neurosci* 34:418–433.
33. Barmada SJ, et al. (2015) Amelioration of toxicity in neuronal models of amyotrophic lateral sclerosis by hUPF1. *Proc Natl Acad Sci USA* 112:7821–7826.
34. Tsvetkov AS, et al. (2013) Proteostasis of polyglutamine varies among neurons and predicts neurodegeneration. *Nat Chem Biol* 9:586–592.
35. Skibinski G, et al. (2017) Nrf2 mitigates LRRK2- and α-synuclein-induced neurodegeneration by modulating proteostasis. *Proc Natl Acad Sci USA* 114:1165–1170.
36. Ohrfelt A, et al. (2011) Identification of novel α-synuclein isoforms in human brain tissue by using an online nanoLC-ESI-FTICR-MS method. *Neurochem Res* 36:2029–2042.
37. Martinez-Vicente M, et al. (2008) Dopamine-modified alpha-synuclein blocks chaperone-mediated autophagy. *J Clin Invest* 118:777–788.
38. Gurskaya NG, et al. (2006) Engineering of a monomeric green-to-red photoactivatable fluorescent protein induced by blue light. *Nat Biotechnol* 24:461–465.
39. Okochi M, et al. (2000) Constitutive phosphorylation of the Parkinson's disease associated alpha-synuclein. *J Biol Chem* 275:390–397.
40. Miake H, Mizusawa H, Iwatsubo T, Hasegawa M (2002) Biochemical characterization of the core structure of alpha-synuclein filaments. *J Biol Chem* 277:19213–19219.
41. Burré J, Sharma M, Südhof TC (2012) Systematic mutagenesis of α-synuclein reveals distinct sequence requirements for physiological and pathological activities. *J Neurosci* 32:15227–15242.
42. Tsika E, et al. (2010) Distinct region-specific alpha-synuclein oligomers in A53T transgenic mice: Implications for neurodegeneration. *J Neurosci* 30:3409–3418.
43. Mbefo MK, et al. (2015) Parkinson disease mutant E46K enhances α-synuclein phosphorylation in mammalian cell lines, in yeast, and in vivo. *J Biol Chem* 290:9412–9427.
44. Bergeron M, et al. (2014) In vivo modulation of polo-like kinases supports a key role for PLK2 in Ser129 α-synuclein phosphorylation in mouse brain. *Neuroscience* 256:72–82.
45. Arawaka S, et al. (2006) The role of G-protein-coupled receptor kinase 5 in pathogenesis of sporadic Parkinson's disease. *J Neurosci* 26:9227–9238.
46. Seeburg DP, Feliu-Mojer M, Gaiottino J, Pak DT, Sheng M (2008) Critical role of CDK5 and polo-like kinase 2 in homeostatic synaptic plasticity during elevated activity. *Neuron* 58:571–583.
47. Matsumoto T, et al. (2009) Polo-like kinases mediate cell survival in mitochondrial dysfunction. *Proc Natl Acad Sci USA* 106:14542–14546.
48. Michal AM, et al. (2012) G Protein-coupled receptor kinase 5 is localized to centrosomes and regulates cell cycle progression. *J Biol Chem* 287:6928–6940.
49. Bowers S, et al. (2013) Design and synthesis of highly selective, orally active polo-like kinase-2 (Plk-2) inhibitors. *Bioorg Med Chem Lett* 23:2743–2749.
50. Homan KT, Wu E, Cannavo A, Koch WJ, Tesmer JJ (2014) Identification and characterization of amlexanox as a G protein-coupled receptor kinase 5 inhibitor. *Molecules* 19:16937–16949.
51. Nemani VM, et al. (2010) Increased expression of alpha-synuclein reduces neurotransmitter release by inhibiting synaptic vesicle reclustering after endocytosis. *Neuron* 65:66–79.
52. Selkoe DJ, Hardy J (2016) The amyloid hypothesis of Alzheimer's disease at 25 years. *EMBO Mol Med* 8:595–608.
53. Knafo S, et al. (2016) PTEN recruitment controls synaptic and cognitive function in Alzheimer's models. *Nat Neurosci* 19:443–453.
54. Kasten M, Klein C (2013) The many faces of alpha-synuclein mutations. *Mov Disord* 28:697–701.
55. Zarranz JJ, et al. (2004) The new mutation, E46K, of alpha-synuclein causes Parkinson and Lewy body dementia. *Ann Neurol* 55:164–173.
56. Conway KA, Harper JD, Lansbury PT (1998) Accelerated in vitro fibril formation by a mutant alpha-synuclein linked to early-onset Parkinson disease. *Nat Med* 4:1318–1320.
57. Outeiro TF, Lindquist S (2003) Yeast cells provide insight into alpha-synuclein biology and pathobiology. *Science* 302:1772–1775.
58. Fortin DL, et al. (2004) Lipid rafts mediate the synaptic localization of alpha-synuclein. *J Neurosci* 24:6715–6723.
59. Emmer KL, Waxman EA, Covy JP, Giasson BI (2011) E46K human alpha-synuclein transgenic mice develop Lewy-like and tau pathology associated with age-dependent, detrimental motor impairment. *J Biol Chem* 286:35104–35118.
60. Cannon JR, et al. (2013) Expression of human E46K-mutated α-synuclein in BAC-transgenic rats replicates early-stage Parkinson's disease features and enhances vulnerability to mitochondrial impairment. *Exp Neurol* 240:44–56.
61. Lee Y, Dawson VL, Dawson TM (2012) Animal models of Parkinson's disease: Vertebrate genetics. *Cold Spring Harb Perspect Med* 2:a009324.
62. Richfield EK, et al. (2002) Behavioral and neurochemical effects of wild-type and mutated human alpha-synuclein in transgenic mice. *Exp Neurol* 175:35–48.
63. Nuber S, et al. (2008) Neurodegeneration and motor dysfunction in a conditional model of Parkinson's disease. *J Neurosci* 28:2471–2484.
64. Janezic S, et al. (2013) Deficits in dopaminergic transmission precede neuron loss and dysfunction in a new Parkinson model. *Proc Natl Acad Sci USA* 110:E4016–E4025.
65. Kramer ML, Schulz-Schaeffer WJ (2007) Presynaptic alpha-synuclein aggregates, not Lewy bodies, cause neurodegeneration in dementia with Lewy bodies. *J Neurosci* 27:1405–1410.
66. Milber JM, et al. (2012) Lewy pathology is not the first sign of degeneration in vulnerable neurons in Parkinson disease. *Neurology* 79:2307–2314.
67. Berg D, et al. (2014) Time to redefine PD? Introductory statement of the MDS task force on the definition of Parkinson's disease. *Mov Disord* 29:454–462.
68. Villar-Piqué A, et al. (2016) Environmental and genetic factors support the dissociation between α-synuclein aggregation and toxicity. *Proc Natl Acad Sci USA* 113:E6506–E6515.
69. Winner B, et al. (2011) In vivo demonstration that alpha-synuclein oligomers are toxic. *Proc Natl Acad Sci USA* 108:4194–4199.
70. McCormack AL, Mak SK, Di Monte DA (2012) Increased α-synuclein phosphorylation and nitration in the aging primate substantia nigra. *Cell Death Dis* 3:e315.
71. Samuel F, et al. (2016) Effects of serine 129 phosphorylation on α-synuclein aggregation, membrane association, and internalization. *J Biol Chem* 291:4374–4385.
72. Oueslati A, Schneider BL, Aebischer P, Lashuel HA (2013) Polo-like kinase 2 regulates selective autophagic α-synuclein clearance and suppresses its toxicity in vivo. *Proc Natl Acad Sci USA* 110:E3945–E3954.
73. Lee KJ, et al. (2011) Requirement for Plk2 in orchestrated ras and rap signaling, homeostatic structural plasticity, and memory. *Neuron* 69:957–973.
74. Wong YC, Krainc D (2017) α-synuclein toxicity in neurodegeneration: Mechanism and therapeutic strategies. *Nat Med* 23:1–13.
75. Tanik SA, Schultheiss CE, Volpicelli-Daley LA, Brunden KR, Lee VM (2013) Lewy body-like α-synuclein aggregates resist degradation and impair macroautophagy. *J Biol Chem* 288:15194–15210.